Nuclear Materials and Energy 36 (2023) 101496

Contents lists available at ScienceDirect

Nuclear Materials and Energy

journal homepage: www.elsevier.com/locate/nme

Determination of mechanical properties of tungsten/steel composites using image based microstructure modelling

Vishnu Ganesh *, Daniel Dorow-Gerspach *, Christian Linsmeier

Forschungszentrum Jülich GmbH, Institut für Energie- und Klimaforschung – Plasmaphysik, 52425 Jülich, Germany

ARTICLE INFO

Keywords:
W/steel composites
OOF2
Image based FEM
RVE homogenization

ABSTRACT

Graded tungsten/steel composite is a potential interlayer to alleviate the thermal expansion mismatch between tungsten (W) armour and steel structure in the first wall (FW) of a future fusion reactor. However, existing thermomechanical finite element (FE) numerical simulations of the FW featuring this graded interlayer have modelled the composites inappropriately by assuming their properties to follow an elementary rule of mixtures; linear interpolation of the properties of W and steel based on the volume content of W. This opens up the question of determining the properties of the composites appropriately. Thus, in this study, a microstructural image based modelling technique is proposed to predict the macroscopic mechanical properties of the composites. As a case study, plasma sprayed W/steel composites of three compositions were investigated. FE simulations of the corresponding microstructures, captured via scanning electron microscopy (SEM), were carried out with the help of an open source code (OOF2) which transforms the SEM images into a 2-dimensional mesh. For the determination of macroscopic mechanical properties, image based finite element (FE) simulations of the mapped mesh were carried out. These simulations were done on microstructures of different physical sizes, including mesoscale and microscale morphological artefacts. Also, for each physical size, several SEM images were captured at different sites in the composites to consider the randomness of the material. FE simulations were conducted at various virtual temperatures between 20 °C and 700 °C. The predicted mechanical properties agreed much better with the few available experimentally determined literature values of the composites than the simple linear interpolation.

1. Introduction

The first wall (FW) of future fusion reactors, shall entail tungsten (W) armour to protect the underlying steel (Eurofer 97) structure. An interlayer made of W/steel composites with gradually varying concentrations of W and steel is expected to compensate for the difference in the coefficient of thermal expansion of W and steel. However, to date, all the thermomechanical finite element (FE) simulation studies have inadequately modelled the composites by assuming their elastic modulus (E) and yield strength (R_p) to be equal to the linear interpolated values of pure W and pure steel [1–4], resulting in an underestimation of stresses and strains in the FW, as stated by Heuer [5]. This rudimentary modelling fails to consider the presence of porosity, the microstructure's morphology, and the individual constituents' phase distribution. To address this issue, a micromechanical modelling technique using microstructural image-based computational FE simulations is proposed to predict the composite's macroscopic mechanical properties. Although the use of modelling the microstructural cross-sections with 2-dimensional (2D) elements constitutes a strong simplification, it was applied and proved valid experimentally on different types of materials like Ti_3SiC_2/SiC composites [6], tailor-tempered 22MnB5 boron steel [7], and plasma sprayed W/CuCrZr composite [8]. Moreover, this technique has been successfully employed for fusion-relevant W based composites [8,9]. This study presents a case study of plasma sprayed W/steel composites [10], whose exemplary microstructures are shown in Fig. 1.

2. Methodology for image based simulation

2.1. Modelling procedure

The procedure for the computational approach is schematically represented in Fig. 2, similar to what is described by Zivelonghi et al. [8]. At first, a high-resolution SEM microstructural image, captured at the cross-section of the composite, underwent necessary image

* Corresponding authors.
E-mail addresses: v.ganesh@fz-juelich.de (V. Ganesh), d.dorow-gerspach@fz-juelich.de (D. Dorow-Gerspach).

https://doi.org/10.1016/j.nme.2023.101496
Received 2 July 2023; Received in revised form 24 August 2023; Accepted 27 August 2023
Available online 28 August 2023

modification steps such as adjusting brightness and contrast and clearing out any background noise to capture all three major constituents, i.e., W, steel and voids. Then, this modified image is incorporated into an open source code called OOF2, which transforms it into a 2D mapped mesh by following an algorithm, as depicted in Fig. 2 [11,12]. The final mapped mesh consisted of 6 noded-triangular and 8 noded-quadrilateral quadratic elements, an exemplary mesh is shown in Fig. 3. Detailed information regarding the fundamentals of each operation listed in this algorithm for mesh generation is provided in the OOF2 manual [13].

Element formulation: This mapped mesh is imported into a commercial FE solver (ANSYS). The mesh generated through OOF2 often contains some badly shaped elements with a high aspect ratio. However, if the number of these elements is less than 0.1 % of the total number of elements, the presence of such elements could lead to a convergence issue. Thus, higher order plane-stress elements (PLANE183) utilizing quadratic shape function are used for the modelling. This element type is suitable for modelling irregular meshes and large deformations as it shows a better convergence of the solution. The selection of plane-stress elements was based on the previous studies by Zivelonghi [14] on the microstructural image based modelling of W/CuCrZr composites of two compositions (30 vol% W and 70 vol% W), which states that a plane-stress condition predicts a realistic behavior and the computed tensile stress–strain curves were close to that of the experimental results.

Material modelling: W and steel were modelled as isotropic elastic–-plastic materials, with elastic behaviour following Hooke's law and the plastic yield surface following von Mises yield criterion. The plastic flow curve for W was modelled as linearly constant, while for steel it follows an isotropic Voce strain hardening law. The temperature-dependent elastic modulus and initial flow stress (yield strength) of W and steel were taken from ITER and EUROfusion materials property handbooks, respectively [15,16]. The temperature-dependent flow curve for steel was taken from available stress–strain curves in literature [17].

Boundary condition: As mentioned earlier, the FGM is considered an interlayer, and the thermal stresses during the operation of the reactor arise due to the difference in the CTE mainly along the x-direction (see Fig. 4). Thus, the microstructure is deformed along the x-direction, which is also along the lamellar direction of such plasma sprayed composites. So, a global strain of 2 % is applied on the face CD, as schematically represented by exemplary applied boundary conditions on one such microstructure in Fig. 4. In the field of computational materials science, this microstructure (cuboid ABCD) is called a representative volume element (RVE), as this is the volume on which computational simulation is performed.

Solver: The simulation is solved using an implicit sparse direct solver to overcome any convergence issue by considering an unsymmetrical stiffness matrix for non-linear problems. All the computation was performed on a Dell Precision 3630 Workstation with Intel(R) Core i7-9700 3.0 GHz on 8 physical CPU cores containing 64 GB Memory.

2.2. Methodology to determine macroscopic property

The simulation of a tensile test on one RVE outputs the reaction forces at the boundary conditions, as shown in Fig. 4. A stress–strain response is generated from these reaction forces, which is analogous to a virtual tensile test performed on that particular RVE at different virtual temperatures. From the stress–strain response, temperature dependent E and R_p can be determined. The size of the RVE (microstructure) strongly influences the output mechanical property. It is common to think that a large size RVE would predict a more realistic behavior of the material; this is only true if the SEM image captures all morphological artefacts correctly. A larger size RVE represents results from a SEM micrograph taken at lower magnification. This SEM micrograph cannot capture microscale inclusions/shapes/voids. It would be only able to capture patterns that are sufficiently large enough. A smaller size RVE represents a SEM micrograph captured at higher magnification. This SEM micrograph would capture all microscale morphological patterns. However, it may not represent the overall pattern of the composite. Thus, in this study, the modelling is performed on microstructures of different physical sizes depending on the composition, as shown in Fig. 5. To get a better statistical response of the macroscopic mechanical property, a minimum of two randomly selected SEM micrographs had been taken for each RVE size, as shown in Fig. 5. So, for instance, for a 25W composition, in total 15 simulations corresponding to 15 micrographs were performed at each virtual temperatures. From each microstructure, the macroscopic property (E^i, R_p^i) and then a mean homogenized property was obtained, according to the methodology shown in Fig. 5. This represents the macroscopic mechanical property of that particular composite.

3. Results and discussion

3.1. Deformation behaviour

The deformation mechanism in the plasma sprayed composites was understood using accumulated equivalent strain fields of the FE simulation. To respect the article's length, these strain fields are provided in supplementary material A and only a gist is provided here. The deformation occurred due to the local strain concentration at narrows in the microstructure initiating at voids/pores, as these sites act as stress concentration spots. Upon further global deformation, the strain accumulates near these sites and forms bands. It was observed that the thin gaps/voids between two adjacent splats also act as failure initiation sites. These bands are predominately formed along the boundaries between W and steel upon further increase of the global strain. These bands then join other bands originating from other voids/failure sites. Then these interconnected bands run through the entire microstructure, and the axis of them is oriented perpendicular to the global tensile direction. In the 25W composite, most of the plastic strain localised in

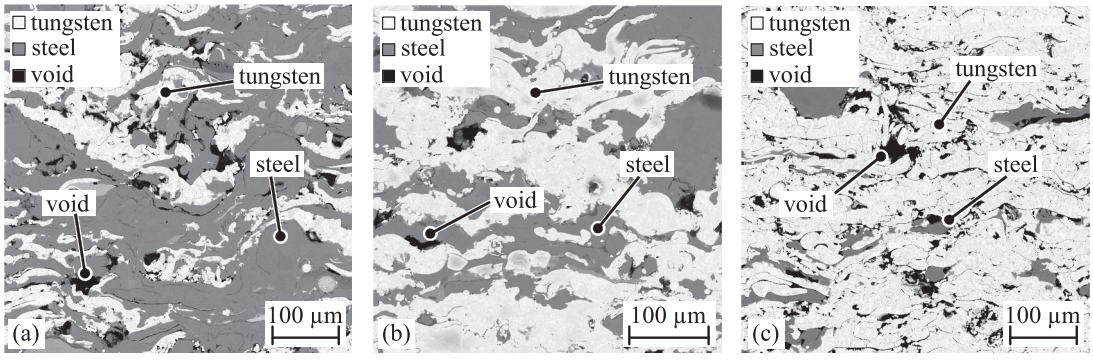

Fig. 1. Exemplary scanning electron microscopy (SEM) micrographs of the plasma sprayed composites of three compositions: (a) 25W, (b) 50W and (c) 75W (*Note: 25W refers to a composition with 25 vol% W and 75 vol% steel*).

steel, and it was observed that this severe plastic straining exceeds the rupture strain of the steel. Some minor plastic strain localizations were also observed in the W phase, but these were rare. In the 50W composite, the deformation mechanism was similar to what was observed in 25W. However, the accumulation of plastic strain was also observed in W. In 75W composite, the presence of steel phase is significantly less, and the 75W composites were highly porous (~9 % [10]). Plastic straining in steel was not observed as there is very little steel. This 75W composite shows pores between two adjacent W splats, and it was observed that the failure occurs mainly at these sites. The plastic strain accumulated at these sites follows/propagates along the boundaries of the intersplat porosities leads to a complete rupture of the composite.

3.2. Macroscopic mechanical property

After performing all the FE simulations on various RVE, the resultant mean homogenized property is determined, as shown in Fig. 6. The graph shows the output data points (E and R_p) obtained from FE simulations on each microstructure. It is compared with the few available experimentally determined macroscopic mechanical properties of the composites in some literatures. The experimentally determined elastic modulus obtained via resonance ultrasound spectroscopy (RUS) is plotted in Fig. 6 [18]. The experimentally determined flexural yield strength of the composites obtained via a miniature 4-point bending test is also plotted alongside [19]. The simple linear interpolation of elastic modulus (E_{linear}) and yield strength ($R_{p,linear}$) for all three compositions are plotted alongside for comparison. Based on the results obtained, some key discussions are made as follows. First, one should note the

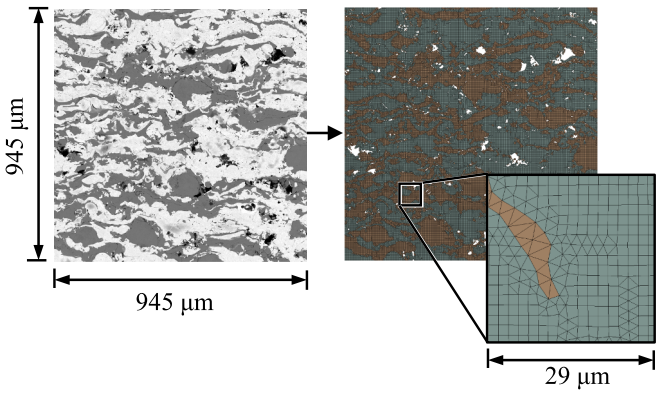

Fig. 3. An exemplary mapped mesh from a SEM image for a 50W composite taken at a random location consisting of 2048 pixel × 2048 pixel. This had a geometric size of 945 µm × 945 µm. On the left SEM image, grey represents steel, white represents W, and black represents voids. This mapped mesh consisted of 366,439 elements with 941,421 nodes.

considerable amount of scattering of the simulation outputs. This illustrates the inhomogeneity of plasma sprayed composites and that the usage of several locations and magnifications of the microstructures was important. Second, looking at the two different models (simple linear interpolation and mean homogenized), it can be seen that only in the case of the elastic modulus of 50W, they are comparatively close to each other. The exact reason for this surprising behaviour is still not clear, but it could be attributed to its low porosity (~4 %) and poor interlamellar

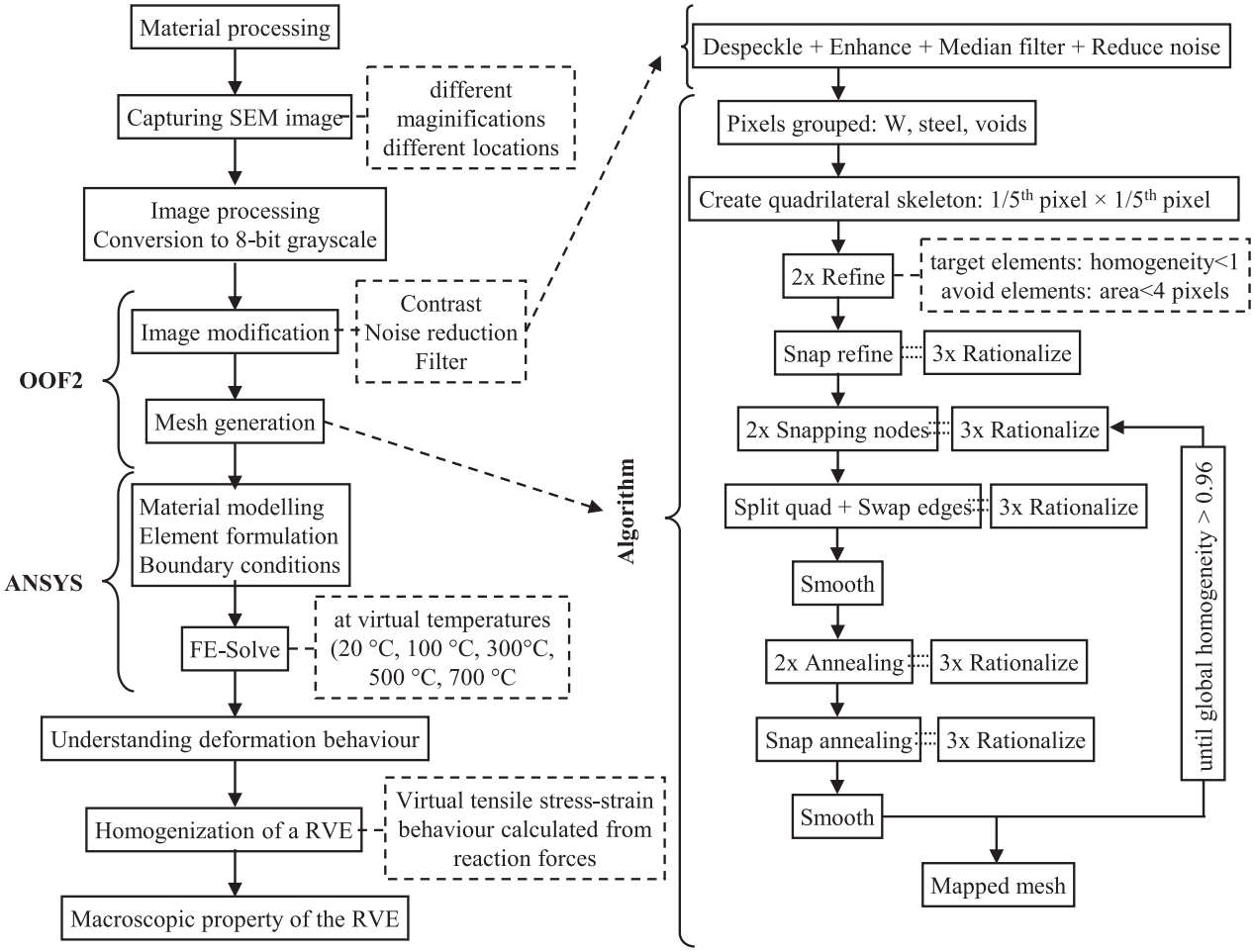

Fig. 2. Procedure for one microstructural image (one representative volume element).

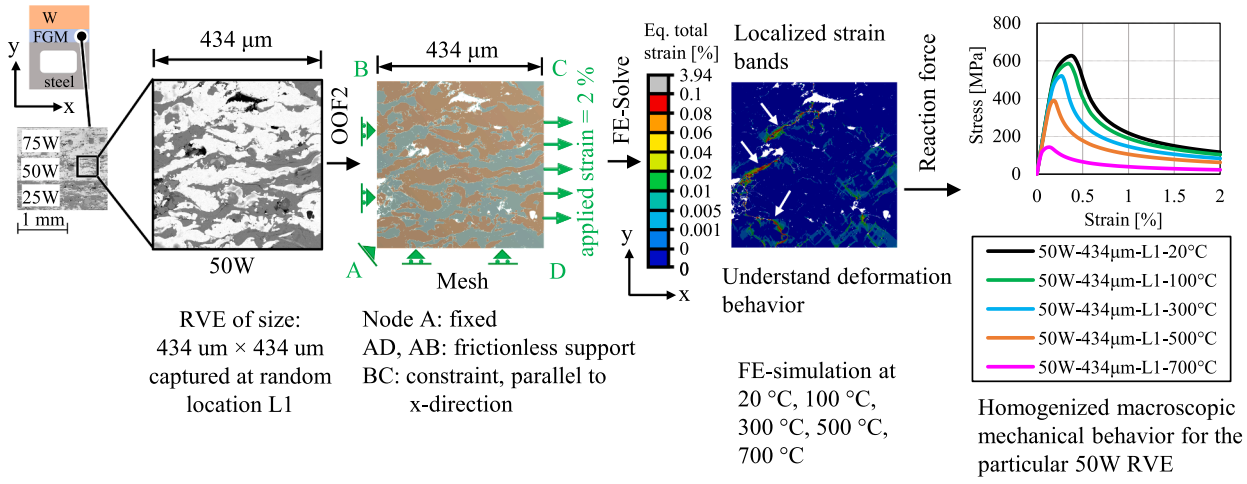

Fig. 4. Exemplary depiction of macroscopic stress–strain response of a particular 50W microstructural representative volume element (RVE); showing the direction along which the micromechanical simulation is performed and applied boundary condition depicted schematically.

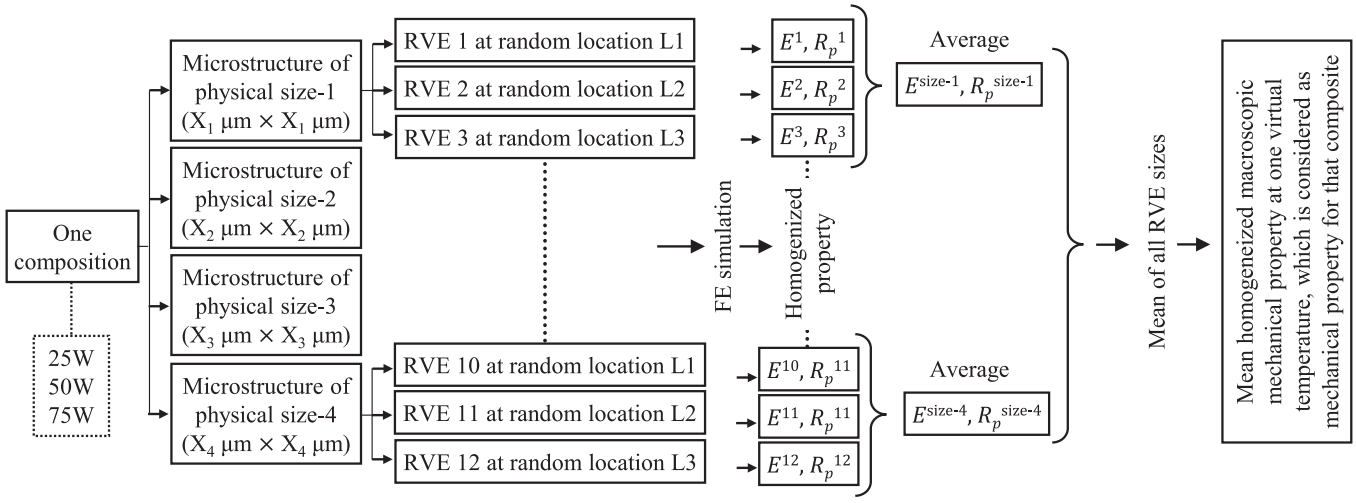

Fig. 5. Schematic representation of the methodology for the determination of homogenized macroscopic mechanical property.

bonding which is assumed to be perfect in the simulation. Moreover, the different mechanical properties of plasma sprayed W and steel assumed in the simulation compared to their counterparts taken from the ITER and EUROfusion materials property handbooks could also play a significant role as well. Likewise, the 50W exhibits only half the porosity (~4 %) than the other two compositions (25W ~7 % and 75W ~9 %) [10]. This is for sure one important aspect for this behaviour surprising behaviour. As it, most probably, also accounts for the lower scattering seen in the data. Third, for the other two compositions (25W and 75W) the mean homogenised elastic modulus properties are much lower than the linear interpolated values, and thereby, in quite good agreement to the few available experimentally values. Also, the yield stress of all composites predicted by the mean homogenized shows a good agreement with the few measurements. This shows that despite the simplifying assumptions in 2D RVE modelling, the method used in this study can significantly improve the theoretical prediction. It also illustrates that taking the real microstructure and its shortcomings into account can already explain much of the worse mechanical properties when comparing the measured values and the initial expectation from linear interpolation. Fourth, the experimentally obtained properties show a non-monotonic dependence on the W content. The simulation model was also able to predict this non-monotonic behaviour, which could—at this moment—be attributed to the following traits: presence of porosity, inadequate metallurgical adhesion among the adjacent splats, and presence of microscale voids between two adjacent splats.

4. Conclusion

In this study a microstructure image-based FE simulation technique to predict the composite's homogenized macroscopic mechanical properties is presented. As a case study, plasma sprayed W/steel composite of three different compositions was considered, which has a potential application field in the FW. The methodology suggests simulation on the microstructure of different physical sizes to incorporate mesoscale and microscale morphological artefacts. The inhomogeneity of the microstructure was considered by performing the FE simulations on microstructural images taken at different randomly chosen locations. The predicted mean homogenized macroscopic property of the composite agrees much better with the experimentally measured literature values than the simple linear interpolation. The modelling technique also points out the locations of possible failure, namely the initiation and propagation of bands of concentrated plastic deformation. The study suggests that this modelling technique could be used for such composites, providing a more realistic estimation of the stresses inside the graded FW. More experimental data including their temperature dependency is needed to further improve the model and the assessment of

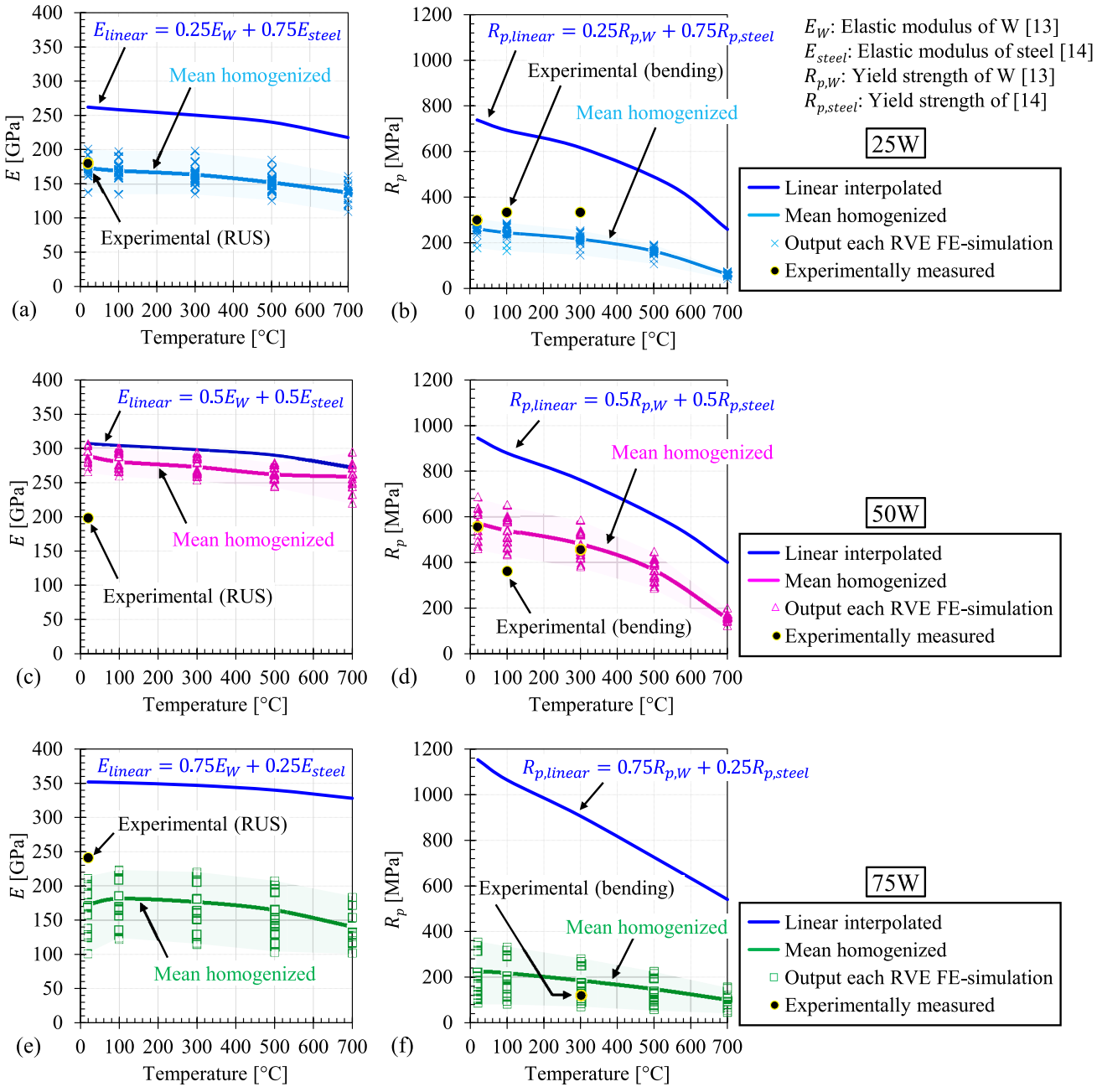

Fig. 6. Homogenized macroscopic mechanical properties (elastic modulus and yield strength) of three compositions: a), b) 25W; c), d) 50W; e), f) 75W; these are compared with experimentally determined literature value of elastic modulus via RUS method and experimentally determined literature value of yield strength via miniature 4-point bending test; also, linearly interpolated values are plotted alongside for comparison.

its quality.

CRediT authorship contribution statement

Vishnu Ganesh: Conceptualization, Methodology, Formal analysis, Investigation, Writing – original draft. **Daniel Dorow-Gerspach:** Supervision, Writing – review & editing, Funding acquisition. **Christian Linsmeier:** Supervision.

Declaration of Competing Interest

The authors declare that they have no known competing financial interests or personal relationships that could have appeared to influence the work reported in this paper.

Data availability

No data was used for the research described in the article.

Acknowledgement

The authors would like to thank Stefan Kirtz for his assistance in setting up the simulation hardware; Jiri Matejicek, Monika Vilemova, Marek Janata and Zdenek Kutilek for their assistance in plasma spraying; Jan Coenen, Gerald Pintsuk and Marius Wirtz (the project leaders at FZJ); and Simon Heuer. This work has been carried out within the framework of the EUROfusion Consortium, funded by the European Union via the Euratom Research and Training Programme (Grant Agreement No 101052200 — EUROfusion). Views and opinions

expressed are however those of the author(s) only and do not necessarily reflect those of the European Union or the European Commission. Neither the European Union nor the European Commission can be held responsible for them.

Appendix A. Supplementary data

Supplementary data to this article can be found online at https://doi.org/10.1016/j.nme.2023.101496.

References

[1] T. Emmerich, D. Qu, R. Vaßen, J. Aktaa, Development of W-coating with functionally graded W/EUROFER-layers for protection of First-Wall materials, Fusion Eng. Des. 128 (2018) 58–67, https://doi.org/10.1016/j.fusengdes.2018.01.047.

[2] T. Weber, J. Aktaa, Numerical assessment of functionally graded tungsten/steel joints for divertor applications, Fusion Eng. Des. 86 (2011) 220–226, https://doi.org/10.1016/j.fusengdes.2010.12.084.

[3] D. Qu, W.W. Basuki, J. Aktaa, Numerical assessment of functionally graded tungsten/EUROFER coating system for first wall applications, Fusion Eng. Des. 98–99 (2015) 1389–1393, https://doi.org/10.1016/j.fusengdes.2015.06.120.

[4] S. Heuer, T. Weber, G. Pintsuk, J.W. Coenen, J. Matejicek, C. Linsmeier, Aiming at understanding thermo-mechanical loads in the first wall of DEMO: stress-strain evolution in a Eurofer-tungsten test component featuring a functionally graded interlayer, Fusion Eng. Des. 135 (2018) 141–153, https://doi.org/10.1016/j.fusengdes.2018.07.011.

[5] S. Heuer, Charakterisierung gradierter Eisen/Wolfram-Schichten für die erste Wand von Fusionsreaktoren. PhD dissertation, Bochum, Germany, 2017.

[6] B.N. Nguyen, C.H. Henager Jr., R.J. Kurtz, A dual-phase microstructural approach to damage and fracture of Ti3SiC2/SiC joints, J. Nucl. Mater. 499 (2018) 496–503, https://doi.org/10.1016/j.jnucmat.2017.11.054.

[7] B. Tang, Q. Wang, N. Guo, J. Liu, H. Ge, Z. Luo, X. Li, Microstructure-based RVE modeling of ductile failure induced by plastic strain localization in tailor-tempered 22MnB5 boron steel, Eng. Frac. Mech. 240 (2020), 107351, https://doi.org/10.1016/j.engfracmech.2020.107351.

[8] A. Zivelonghi, A. Brendel, S. Lindig, S. Nawka, B. Kieback, J.-H. You, Microstructure-based analysis of thermal- and mechanical behaviors of W/CuCrZr composites and porous W coating, J. Nucl. Mater. 417 (2011) 536–539, https://doi.org/10.1016/j.jnucmat.2010.12.256.

[9] B.N. Nguyen, C.H. Henager Jr., J. Wang, W. Setyawan, Tailoring ductile-phase toughened tungsten hierarchical microstructures for plasma-facing materials, J. Nucl. Mater. 540 (2020), 152382, https://doi.org/10.1016/j.jnucmat.2020.152382.

[10] V. Ganesh, D. Dorow-Gerspach, S. Heuer, J. Matejicek, M. Vilemova, M. Bram, J. W. Coenen, M. Wirtz, G. Pintsuk, W. Theisen, C. Linsmeier, Manufacturing of W-steel joint using plasma sprayed graded W/steel-interlayer with current assisted diffusion bonding, Fusion Eng. Des. 172 (2021), 112896, https://doi.org/10.1016/j.fusengdes.2021.112896.

[11] A.C. Reid, S.A. Langer, R.C. Lua, V.R. Coffman, S.-I. Haan, R.E. García, Image-based finite element mesh construction for material microstructures, Comput. Mater. Sci 43 (2008) 989–999, https://doi.org/10.1016/j.commatsci.2008.02.016.

[12] S.A. Langer, E.R. Fuller, W.C. Carter, OOF: an image-based finite-element analysis of material microstructures, Comput. Sci. Eng. 3 (2001) 15–23, https://doi.org/10.1109/5992.919261.

[13] S.A. Langer, A.C. Reid, V.R. Coffman, G. Dogan, S.-I. Haan, R.E. Garcia, R.C. Lua, The OOF2 Manual: Revision 4.1.0 for OOF2 Version 2.1.17. https://www.ctcms.nist.gov/~langer/oof2man/.

[14] A. Zivelonghi, Thermomechanical Behaviour of Two Heterogenous Tungsten Materials via 2D and 3D Image-based FEM, München, Germany, 2011. PhD dissertation.

[15] ITER, Materials Properties Hanbook (MPH): ITER Doc. G74 MA 16 04-05-07 R0.1., 2017.

[16] EUROfusion, DEMO Material Property Handbook (MPH): EUROFER 97.

[17] M. Rieth, High temperature materials, Karlsruhe, 2008.

[18] S. Heuer, J. Matejicek, M. Vilemova, M. Koller, K. Illkova, J. Veverka, T. Weber, G. Pintsuk, J.W. Coenen, C. Linsmeier, Atmospheric plasma spraying of functionally graded steel/tungsten layers for the first wall of future fusion reactors, Surf. Coating Tech. 366 (2019) 170–178, https://doi.org/10.1016/j.surfcoat.2019.03.017.

[19] V. Ganesh, Joining of Tungsten and Steel for the First Wall of Future Fusion Reactor: (Under Submission). PhD Dissertation, Bochum, Germany, 2023.